Supporting Information

Elucidating the Structure-Performance Relationship in Single-Particle NCM Cathodes *via* Controlled Precursor Synthesis

Soonhyun Hong,[†a] Heesang Lee,[†a] Jahun Koo,[a] Wonchan Hwang,[b] Ji Hwan Kim,[bcd] Yung-Eun Sung,[cd] Jungjin Park,[*b] Young-Sang Yu [*ef] and Chunjoong Kim [*a]

[a] Department of Materials Science and Engineering, Chungnam National University, 99 Daehak-ro, Yuseong-gu, Daejeon 34134, Republic of Korea

[b] Energy Storage Research Center, Clean Energy Research Division, Korea Institute of Science and Technology (KIST), 5 Hwarang-ro, Seongbuk-gu, Seoul 02792, Republic of Korea

[c] Center for Nanoparticle Research, Institute for Basic Science (IBS), Seoul 08826, Republic of Korea

[d] School of Chemical and Biological Engineering, Seoul National University, Seoul 08826, Republic of Korea

[f] Department of Physics, Chungbuk National University, 1 Chungdae-ro, Seowon-gu, Cheongju 28644, Republic of Korea

[g] Advanced Energy Research Institute, Chungbuk National University, 1 Chungdae-ro, Seowon-gu, Cheongju 28644, Republic of Korea

*Corresponding authors

E-mail addresses: jpark716@kist.re.kr (J. Park), youngsang@chungbuk.ac.kr (Y.-S. Yu),_ckim0218@cnu.ac.kr (C. Kim)

	Ni (%)	Co (%)	Mn (%)	Error (ΔNi%)
Target	**92**	**3**	**5**	**-**
pre-1.0/11.2	91.21	3.51	5.28	0.86
pre-2.0/12.1	91.32	3.41	5.27	0.74
pre-5.0/12.1	91.60	3.27	5.13	0.44

Table S1. ICP-derived transition-metal composition (Ni/Co/Mn atomic fractions) of the precursors.

	BET surface area (m^2/g)	BJH Adsorption cumulative volume of pores (cm^3/g)
pre-1.0/11.2	12.0856	0.037170
pre-2.0/12.1	8.0514	0.013563
pre-5.0/12.1	4.6153	0.008287

Table S2. BET specific surface area and total pore volume of the precursors.

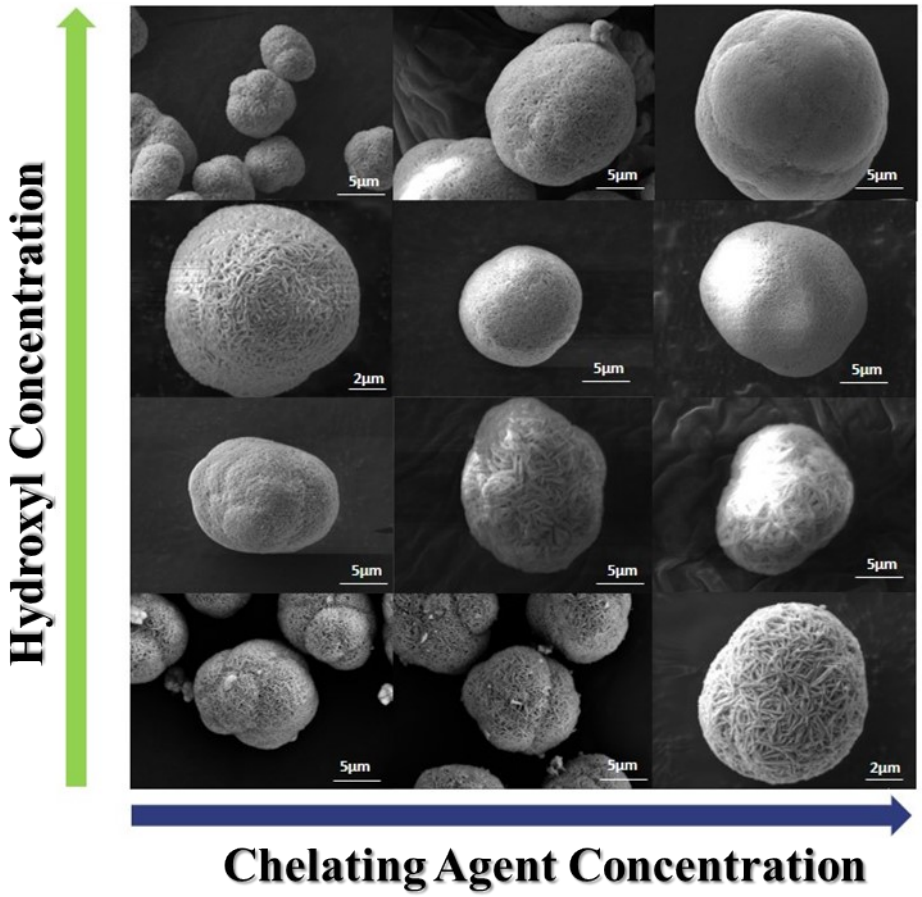

Fig. S1. Summarized scanning electron microscopy (SEM) images of $Ni_{0.92}Co_{0.03}Mn_{0.05}(OH)_2$ precursors with varying hydroxyl and chelating agent concentrations.

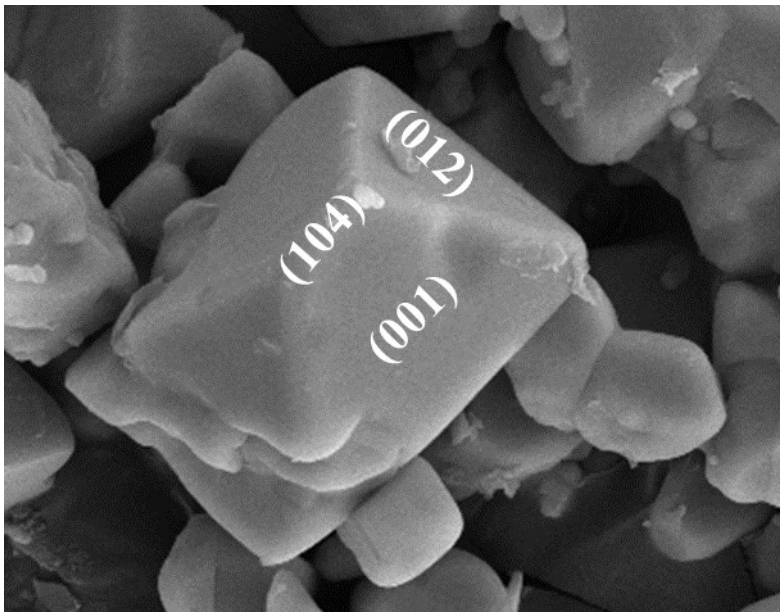

Fig. S2. Representative SEM image of SP-2.0/12.1 sample, showing the well-defined facets on a single particle.

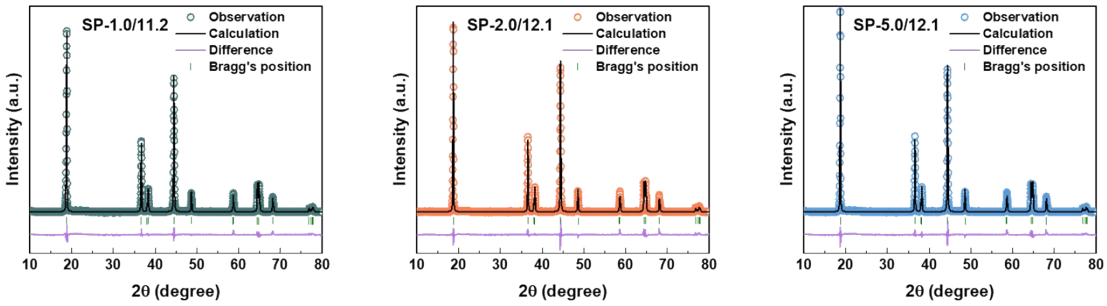

	a (Å)	c (Å)	Volume (Å^3)	Li/TM cataion mixing (%)	GOF
SP-1.0/11.2	2.87469	14.19346	101.578	3.61	5.86
SP-2.0/12.1	2.87529	14.1948	101.63	4.49	6.52
SP-5.0/12.1	2.87472	14.1952	101.593	4.14	6.68

Fig S3. Figure S3. Rietveld refinement of XRD patterns for the three SP-NCM samples, including the refinement plots and the extracted lattice parameters and Li/Ni cation-mixing values.

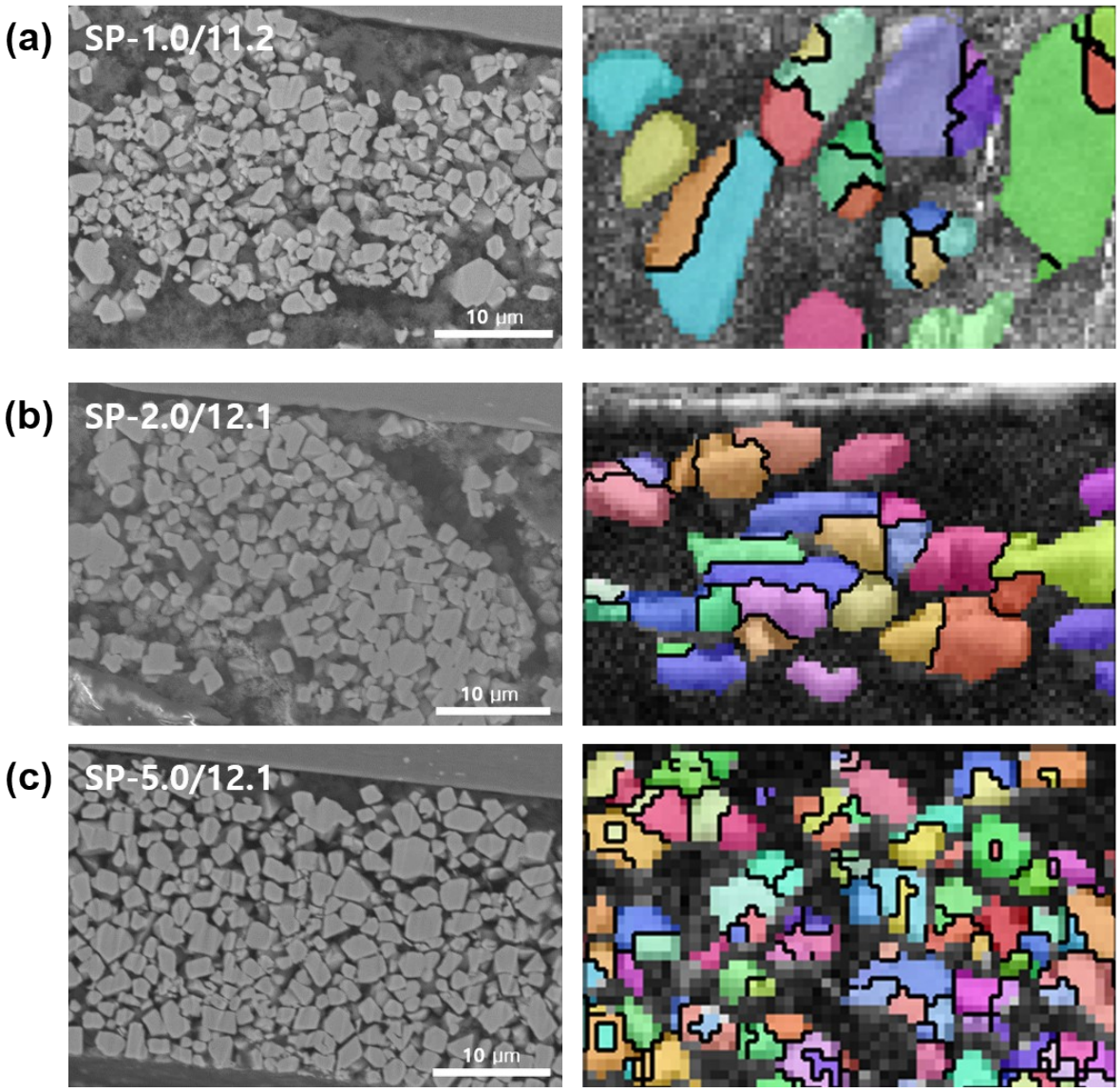

Fig S4. Cross-sectional SEM images and EBSD domain maps of (a) SP-1.0/11.2, (b) SP-2.0/12.1, and (c) SP-5.0/12.1.

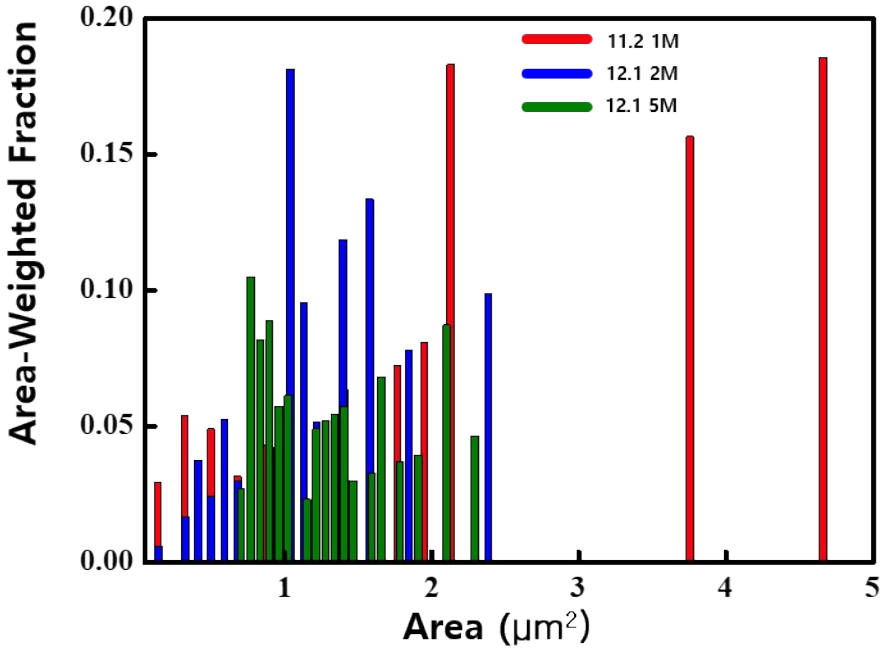

	Area-weight. Mean (μm²)
11.2 1M	2.522
12.1 2M	1.303
12.1 5M	1.288

Fig S5. EBSD domain-size distributions (area vs. area-weighted fraction) for the three samples, with a summary table of the area-weighted mean domain area.

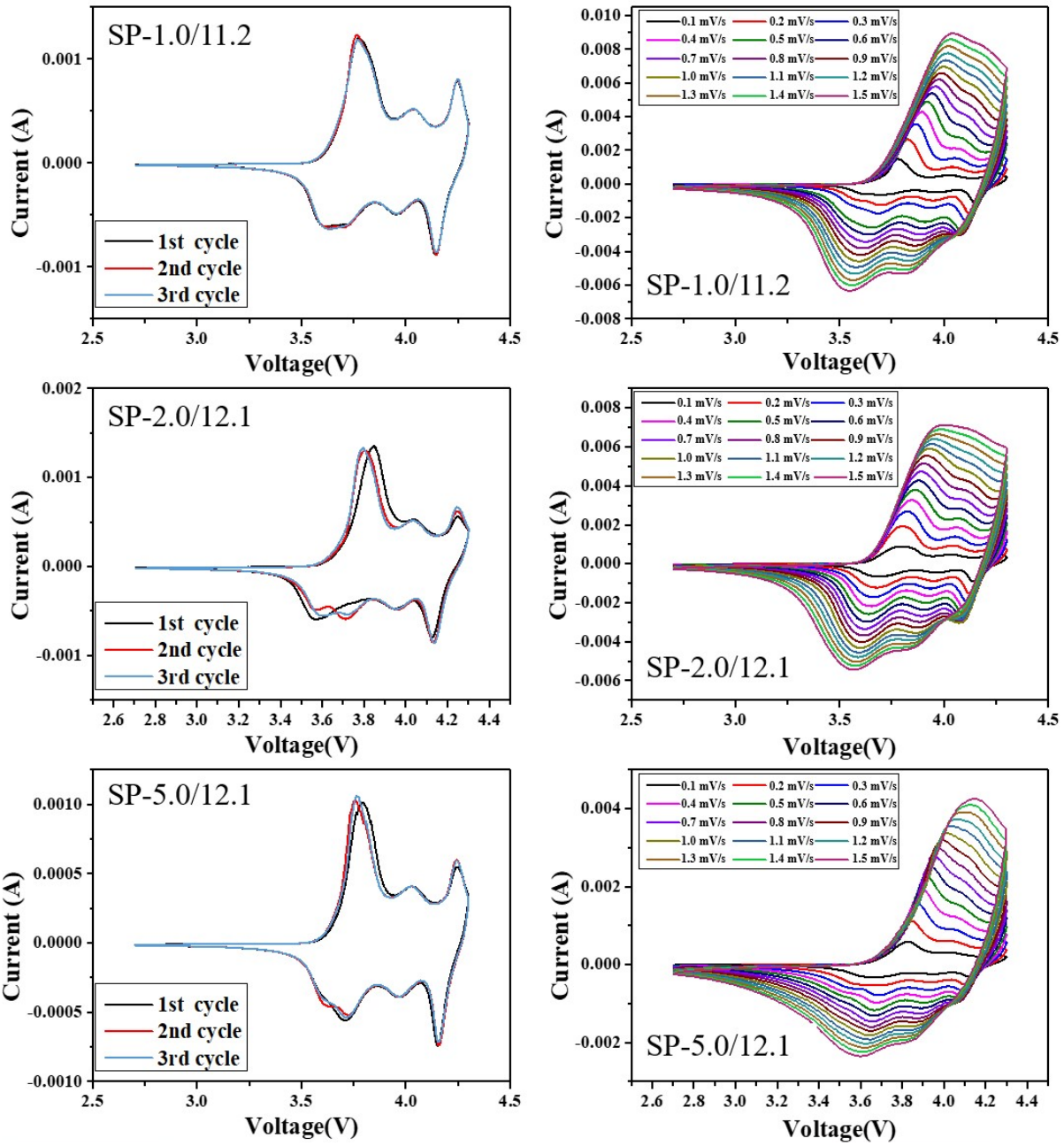

Fig. S6. Cyclic voltammetry (CV) curves of all SP-NCMs for the first three cycles at a fixed scan rate of 0.1 mV/s (left) and with varying scan rates (right).

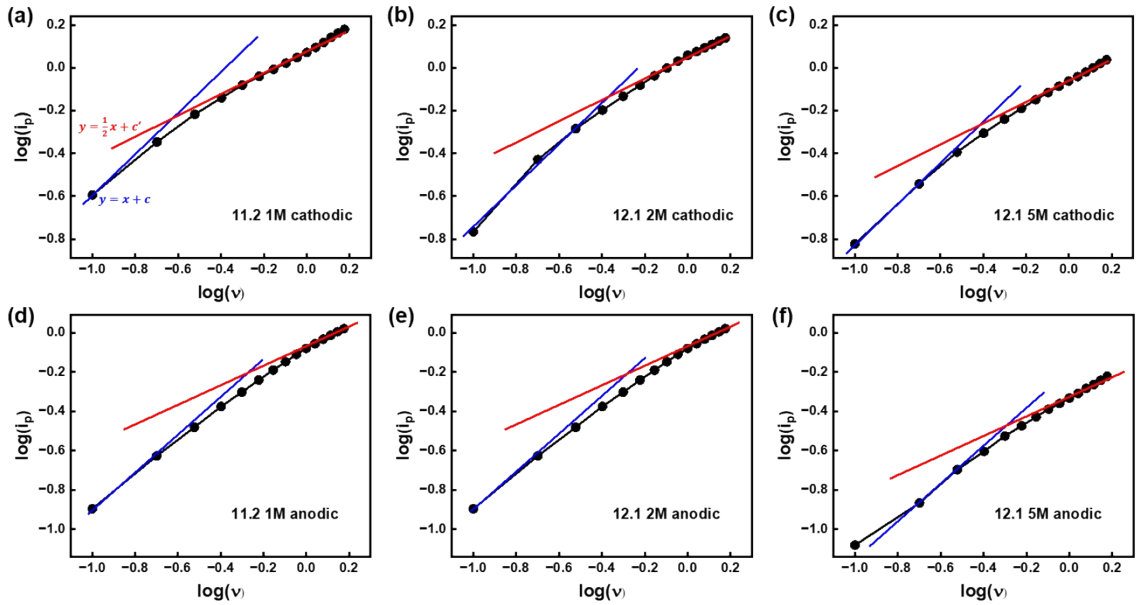

Fig S7. Log–log plots of peak current versus scan rate (log i_p vs. log ν) for (a) SP-1.0/11.2 cathodic, (b) SP-2.0/12.1 cathodic, (c) SP-5.0/12.1 cathodic, (d) SP-1.0/11.2 anodic, (e) SP-2.0/12.1 anodic, and (f) SP-5.0/12.1 anodic peaks; the fitted slopes b in $i_p=a\nu^b$ are indicated.

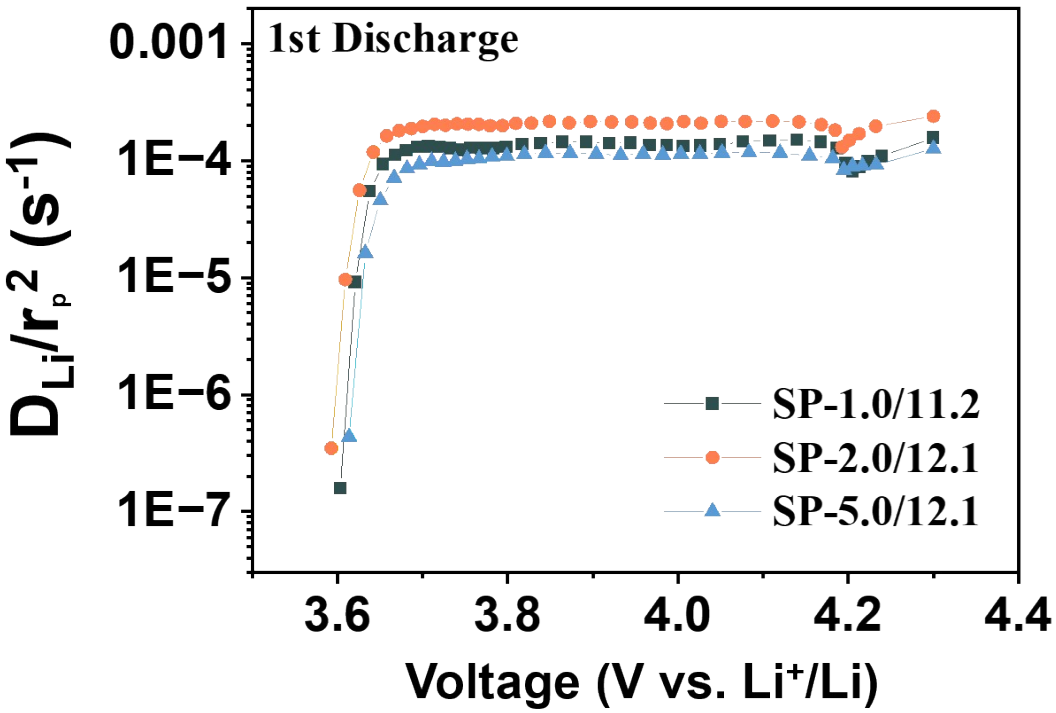

Fig S8. Normalized GITT-derived Li^+ diffusion metric (D/r_p^2) for the three SP-NCM samples.

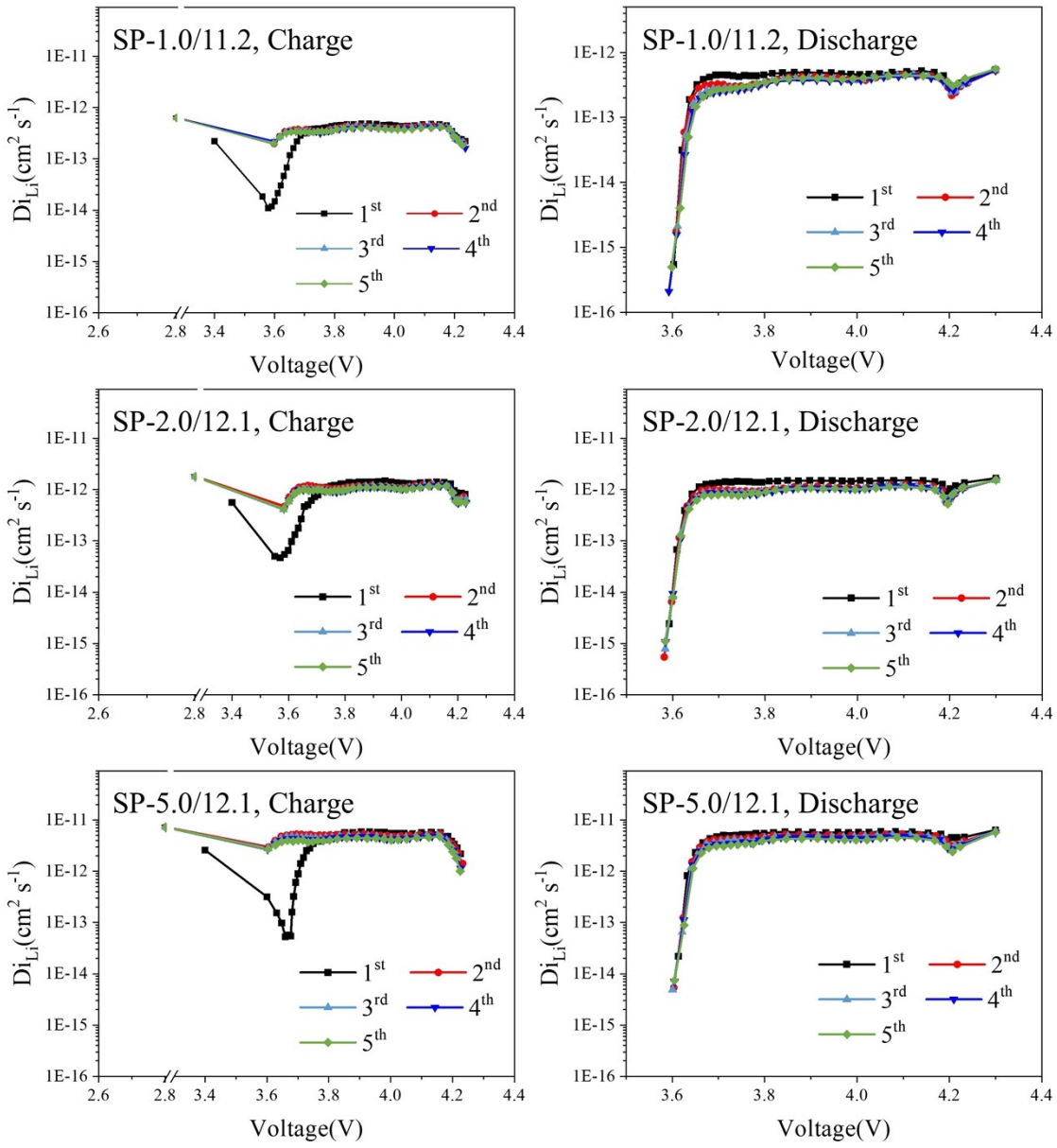

Fig. S9. Galvanostatic intermittent titration technique (GITT) curves of all SP-NCMs during the first five cycles.